

Experimental testing on emulative connections for precast columns using grouted corrugated steel sleeves

Viorel Popa · Andrei Papurcu · Dragos Cotofana · Radu Pascu

Received: 6 August 2014 / Accepted: 6 December 2014 / Published online: 19 December 2014
© Springer Science+Business Media Dordrecht 2014

Abstract Seismic analysis of precast concrete structures requires specific information regarding the behaviour of the connections under large deformation cycles. If a connection is located within the critical region of a structural element, its energy dissipation capacity needs to be confirmed by experimental testing. The use of emulative connections for precast elements is attractive for designers because common conventional design methodologies and assumptions developed for cast in place structures may be readily used. The results of a structural testing program for precast columns connected using grouted corrugated steel sleeves are reported in this paper. A comparison with reference “cast in place” specimens is made and conclusions regarding the emulative characteristic of the connection are drawn. Tests were carried out on scaled concrete columns using the reaction frame at the Technical University of Civil Engineering of Bucharest. Four precast specimens and two reference specimens were tested. Analysis of the recorded data showed that the precast specimens have similar hysteretic response and energy dissipation capacity as the reference ones.

Keywords Structural testing · Emulative detailing · Grouted sleeves · Column-to-foundation connection · Precast concrete

1 Introduction

A wide experience is available worldwide regarding the seismic behaviour of engineered cast in place structures. In many aspects of practical structural analysis and design, consensus among engineering professionals was reached and conventional design methodologies are based on common assumptions. These are stated in design standards and engineers may use them in structural analysis and design. The available information on the seismic behaviour of precast concrete structures is significantly less abundant. The use of proprietary design solu-

V. Popa (✉) · A. Papurcu · D. Cotofana · R. Pascu
Department of Reinforced Concrete Structures, Technical University of Civil Engineering of Bucharest,
Lacul Tei 124, Sector 2, 020396 Bucharest, Romania
e-mail: vpopa@utcb.ro

tions for structural members and connections inhibits the circulation of existing information. Despite the extended practice there is no unitary approach in seismic structural analysis and design of precast structures. Usually, seismic design standards comprise brief provisions for these structures.

Earthquakes that hit regions with moderate or advanced structural engineering practice revealed that precast structures still exhibit weaknesses related mainly to the connections of structural members. Ghosh and Cleland (2012) reported about the collapse of some precast concrete gable frame system warehouses after the 2010 Chilean Earthquake caused by the failure of the welded connections at the drop-in gables. Failure of the column bases caused by improper overlapping of anchor bars with the column bars lacking standard hooks or confinement was also reported. Many authors reported about the poor seismic response of precast concrete buildings in Turkey caused by improper detailing of hinged beams (Posada and Wood 2002; Arslan et al. 2006; Bruneau 2002; Ozden et al. 2014). Liberatore et al. (2013), Bournas et al. (2014) reported about the failure of precast structures due to unseating of beams, failure of lateral restraint of the beam pocket support, tensile failure of steel fasteners at the beam-column connection during the Emilia 2012 earthquake in Italy.

In the design of precast concrete structures two types of jointing details can be conventionally defined with respect to their behaviour in comparison with the monolithic ones (ACI 2009). If precast members are connected using special jointing details, such as bolted or welded flanges, the bending stiffness of the joint differs from that of the member. These joints behave differently from the cast-in-place joints. Their use requires information, including experimental evidence, regarding the behaviour under severe loading conditions especially if the joints are located within the critical regions of beams or columns. This is hardly affordable for regular independent designers or small contractors. The emulative connections are usually wet connections with rebar splices able to restore the monolithic continuity specific to cast-in-place structures. In design, these connections may be regarded as monolithic connections as they have equivalent performance. This way, regularly revised building codes for the design of cast-in-place concrete structures are readily applicable for the design of emulative precast concrete. This makes the design of emulative precast concrete attractive for regular designers. Usually, connections with lapped bars, welded splices or mechanical splices are able to emulate the monolithic cast-in-place behaviour. Their use is tempered by several shortcomings. The use of lapped bars requires a suitable cast-in-place concrete length to accommodate the required lap length. Transverse reinforcement has to be added in the lap length as well. The use of welded splices is not allowed in the critical regions of columns and beams. Mechanical splices can be used in the critical regions only if the strength of the splice is larger than strength of the spliced re-bar (ACI 2011). The use of grouted mechanical couplers requires highly skilled workers and very strict quality control of the grouting process.

Typical precast concrete structures of single-storey commercial or industrial buildings consist of columns embedded in pocket foundations and simply supported beams. This structural layout is widely used worldwide. If the structure is expected to exhibit severe inelastic response under the design earthquake, the foundations are designed based on the flexural capacity of the columns, considering the overstrength. Usually, resulting foundations are large and heavy enough to require a hybrid two-stage construction system: cast-in-place footing with a precast concrete collar on top. This limits the effectiveness of the precast solution as additional construction time is required to complete the foundation. Use of fully cast-in-place foundations, without pockets, is attractive but requires proper solutions for the column to foundation connections. If the jointing is located in the critical regions of the

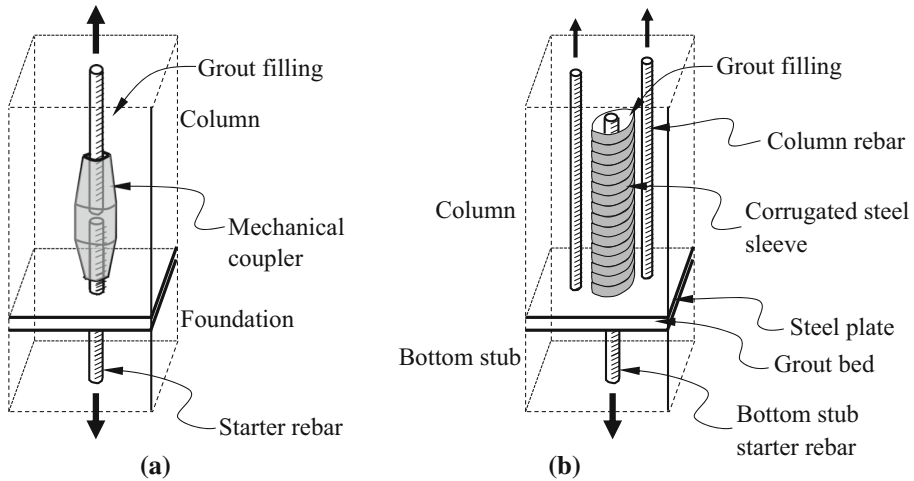


Fig. 1 Rebar splicing using grouted mechanical coupler (a) or grouted corrugated steel sleeve (b)

columns, EN 1998-1 (CEN 2004a, b) requires that the energy dissipation capacity of the connection to be proved by cyclic inelastic experimental tests.

Grouted mechanical couplers (Fig. 1a) developing the full strength of the rebars can be used in the critical regions of columns (ACI 2011). Jointing by lapping rebars using grouted corrugated steel sleeves represents an alternative solution. Limited information about the hysteretic behaviour of such column-to-foundation connections can be found in literature. Belleri and Riva (2012) reported about cyclic behaviour of grouted corrugated steel sleeves connections with partial de-bonding of the reinforcement. Deliberate local de-bonding of the longitudinal reinforcement in the critical region can be used to increase the rotational ductility and to decrease the tensile strain in the reinforcement. Concentration of plastic deformation at one crack location raises concern about the severe tensile strain necessary to accommodate the rotational ductility demand at the base of the column that could lead to fracture of the reinforcing steel.

This paper reports about the hysteretic behaviour of grouted corrugated steel sleeves connections with fully bonded reinforcement as observed from structural testing. This connection system can be used to connect a precast element with a cast-in-place or a precast one. In this experimental testing program, precast cantilever columns were connected to bottom stubs using grouted corrugated steel sleeves. Lap spliced connections of the starter bars form the bottom stubs with the main rebars of the columns were obtained (Fig. 1b). A comparison with reference monolithic specimens is made and conclusions regarding the “emulative” characteristic of this connection system are drawn.

2 Testing program

The experimental testing program included 6 tests, divided in two groups. The first group consisted of two reference specimens, denoted CIP1 and CIP2, representing typical cast-in-place cantilever columns. The second one consisted of four specimens, denoted PC1, PC2, PC3 and PC4, representing precast cantilever columns having the longitudinal rebars jointed using grouted corrugated steel sleeves. All specimens had the same geometry of the concrete section. Each concrete column, having a 390 mm × 390 mm cross-section and

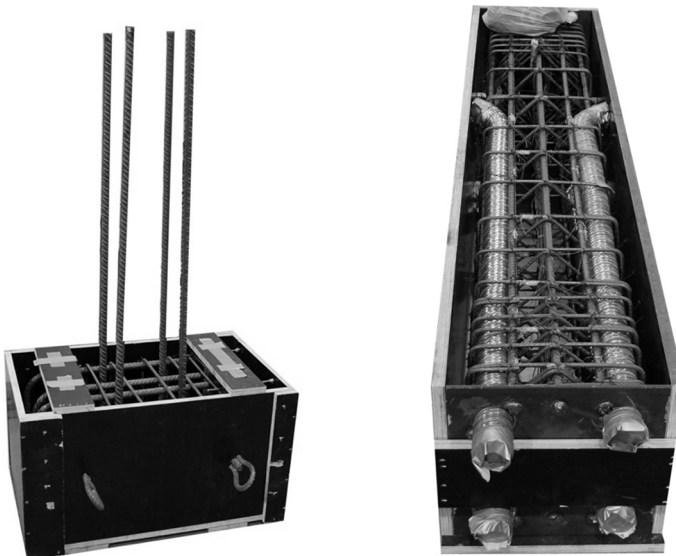
Table 1 Testing program

Specimen	Type	Axial load (kN)
CIP1	Reference/cast in place	1,000
CIP2	Reference/cast in place	2,000
PC1	Precast	1,000
PC2	Precast	1,000
PC3	Precast	2,000
PC4	Precast	2,000

2.00 m clear height, was embedded in a 900 mm × 500 mm × 500 mm bottom stub. The main characteristics of the specimens are briefly presented in Table 1.

Specimens in each group had different connection of the column with the bottom stub. In the first group, continuous longitudinal rebars from the base of the bottom stub to the upper end of the column were installed. At both ends, longitudinal rebars were anchored on perforated steel plates by welding. Concrete was poured in a single stage in these specimens.

In the second group, representing precast columns, corrugated steel sleeves installed in the columns were used to join the longitudinal reinforcement of the columns with the bottom stubs starter bars. In each specimen of the second group concrete was casted in two stages. Initially, the column was casted leaving 4 corrugated steel sleeves placed at the inner corners of the outer stirrup of the column free of concrete. These sleeves were parallel to the longitudinal reinforcement of the column and partially extended on the column height. The sleeves were made of cold-rolled steel ducts made of steel strips commonly used for bonded post-tensioning in prestressed concrete. The bottom stub was casted leaving 4 starter bars in positions matching the column's steel sleeves (Fig. 2). These bars were anchored at the bottom of the stub by welding on a perforated steel plate. After the concrete hardening, the column was lifted up and settled on the bottom stub by inserting the starter bars into the steel sleeves. Using temporary support, a gap of 5 cm was provided between the bottom

**Fig. 2** Bottom stub and precast column prior to concreting

stub and the column. The corrugated steel sleeves and the gap were grouted with shrinkage compensating mortar. A lap-spliced joint between the bottom stub starter bars and the column longitudinal rebars was obtained.

Columns CIP1 and CIP2 were longitudinally reinforced with $4\phi 20$ mm and $4\phi 16$ mm. The $\phi 20$ mm bars were placed at the corners of the outer stirrup. The reinforcement ratio for longitudinal reinforcement was 0.0135. This value is in accordance with the provision of the EN 1998-1 regarding the minimum amount of longitudinal reinforcement in primary seismic concrete columns.

Columns PC1, PC2, PC3 and PC4 were longitudinally reinforced with $12\phi 16$ mm bars. On each side of a column cross-section $3\phi 16$ mm bars were distributed. Four 50 mm in diameter corrugated steel sleeves were placed at the inner corners of the outer stirrup. Each of these sleeves was overlapped with $2\phi 16$ mm rebars. The $12\phi 16$ mm bars correspond to a reinforcement ratio for longitudinal reinforcement of 0.016. Four $\phi 25$ mm starter bars were left out of the bottom stub to be subsequently grouted into the steel sleeves. These bars extended for 1,10 m over the bottom stub. This lap length is in accordance with the provisions of EN 1992-1-1 (CEN 2004a, b) if all the bars are lapped in the same region. The amount of the starter bars was chosen to provide at the bottom section of the columns roughly the same flexural capacity as in case of the reference specimens (CIP). A higher amount of vertical reinforcement was used in the precast specimens in comparison with the cast-in-places ones to compensate for the reduction of the effective depth. Because the steel sleeves were positioned at the inner corners of the outer stirrup, the $\phi 25$ mm starter bars had to be shifted 27 mm towards the centre of the cross-section in comparison with the $\phi 20$ mm rebars of specimens CIP1 and CIP2.

Transverse reinforcement in the columns consisted of pairs of outer and inner $\phi 8$ stirrups, spaced at 50 mm in the critical region at the bottom of the column, 150 mm in the overlapping region of the longitudinal reinforcement and 210 mm elsewhere. Length of the critical region was considered equal to the depth of the cross section of the column, based on EN 1998-1 recommendation for ductility class M. At the upper part of the column, 50 mm spaced stirrups were used to facilitate the load transfer between the reaction beam and the specimen without local damage. A representation of the columns details can be found in Figs. 3 and 4.

Two different axial loads were applied for each group of specimens. Constant axial load of 1,000 kN was applied in the case of specimens CIP1, PC1 and PC2 and 2,000 kN in the case of specimens CIP2, PC3 and PC4. The magnitudes of the axial load were selected to obtain average concrete compressive stresses of approximately $0, 16f_{cd}$ and $0, 32f_{cd}$, where f_{cd} is the design value of the concrete compressive strength defined in EN 1992-1-1. These average compressive stresses in concrete are common for columns of single story industrial warehouses or commercial facilities.

Specimens were designed using concrete class C50/60, according to the definition in EN 1992-1-1 having the characteristic compressive cylinder strength at 28 days of 60 MPa. Concrete compressive strength for each specimen, as observed from material tests in the testing day, and the obtained axial force ratios are given in Table 2. S500 deformed steel bars were used both for transverse and longitudinal reinforcement in the columns and bottom stubs. This steel has the characteristic yield strength of 500 MPa and belongs to class C according to the definition in annex C of EN 1992-1-1. Values of the observed steel tensile strength and strain are given in Table 3. Grouting was done using shrinkage—compensating cement based grout mortar with maximum aggregate size of 3.0 mm, 80 MPa compressive strength at 28 days, having high flow characteristic. Sleeves were manufactured using post-tensioning galvanized steel ducts with corrugated surface. Internal diameter of the duct was 50 mm and thickness of the steel strip was 4 mm.

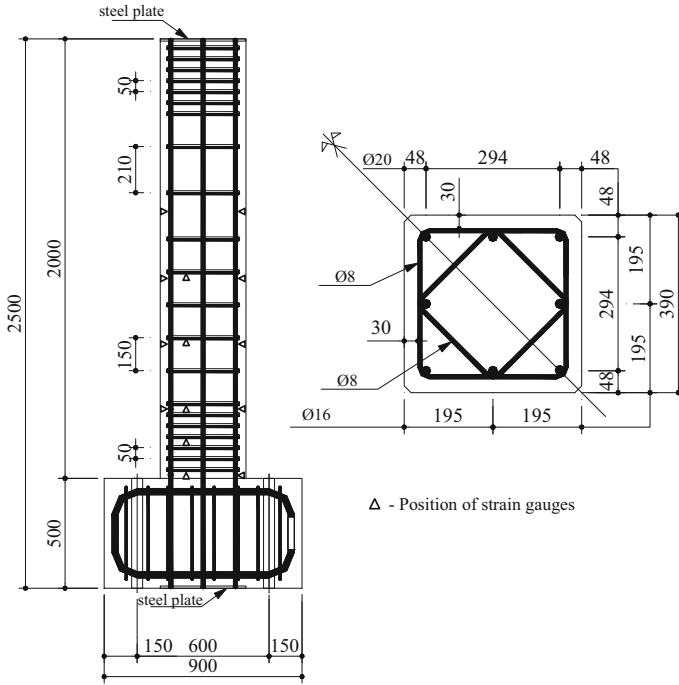


Fig. 3 Layout of reference specimens: CIP1 and CIP2 (all dimensions are in mm)

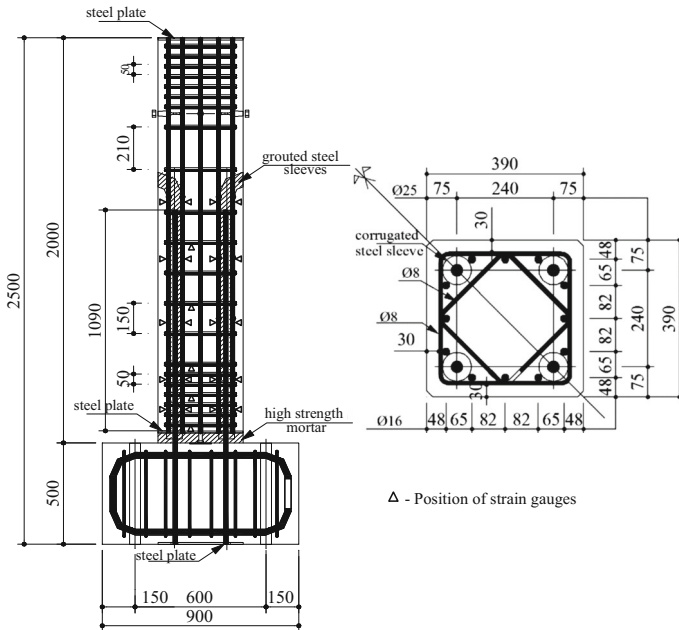


Fig. 4 Layout of specimens PC1, PC2, PC3 and PC4 (all dimensions are in mm)

Table 2 Concrete strength and axial force ratio for each specimen

	f_{cm} (MPa)	f_{ck} (MPa)	f_{cd} (MPa)	N (kN)	ν
CIP1	64.4	56.4	37.6	1,000	0.17
CIP2	70.6	62.6	41.8	2,000	0.31
PC1	60.9	52.9	35.2	1,000	0.19
PC2	70.6	62.6	41.7	1,000	0.16
PC3	70.3	62.3	41.5	2,000	0.32
PC4	70.7	62.7	41.8	2,000	0.31

f_{cm} , observed mean concrete compressive strength; f_{ck} , characteristic compressive strength according to EN1992-1-1; f_{cd} , design compressive strength according to EN1992-1-1; ν , axial force ratio

Table 3 Strength and deformability of steel reinforcement

Φ (Mm)	A_5 (%)	f_{ym} (MPa)	f_{um} (MPa)
25	21.3	533	658
20	24.8	529	670
16	22.9	528	626
8	24.1	550	647

φ , specimen diameter; A_5 , maximum strain measured over a length of 5 diameters; f_{ym} , mean yielding stress; f_{um} , mean tensile strength

All the specimens were tested as vertical cantilevers. They were subjected to displacement based controlled unidirectional lateral load reversals. The drift associated with the yielding, θ_y , was considered to be the deformation control parameter. θ_y was assumed roughly equal to 1.0% for all specimens in order to use the same testing protocol. One loading cycle was performed at $\pm\theta_y/2$ and two loading cycles were performed at $\pm\theta_y$, $\pm 1.5\theta_y$, $\pm 2\theta_y$, $\pm 3\theta_y$, $\pm 4\theta_y$, $\pm 5\theta_y$. This testing protocol (Fig. 5) is consistent with the recommendations of ACI374.2-R13 (ACI 2013) and FEMA461 (FEMA 2007).

Specimens were tested using the reaction frame at the Technical University of Civil Engineering in Bucharest, Romania. The layout of the test setup is presented in Fig. 6. Lateral load was applied using two identical hydraulic jacks with 200 mm maximum stroke and ± 1 MN loading capacity. Constant vertical load was applied using a computer controlled hydraulic jack with 100 mm maximum stroke and 2 MN compression capacity. Load cells were used to measure the horizontal and vertical loads. Pairs of linear displacement transducers were installed to measure the horizontal and vertical displacements between the top of the column and the bottom stub. Strains in longitudinal and transverse reinforcement were measured using electrical strain gauges. Strains in $\varnothing 25$ mm starter bars were not measured. Strain gauges were not installed on these bars in order not to alter the bonding condition with the surrounding mortar due to the presence of electrical wires running continuously parallel to the rebars in the sleeves. Concerns about the ability to fully grout the steel sleeves in the presence of several strain gauges electrical wires existed as well.

Fig. 5 Lateral loading protocol

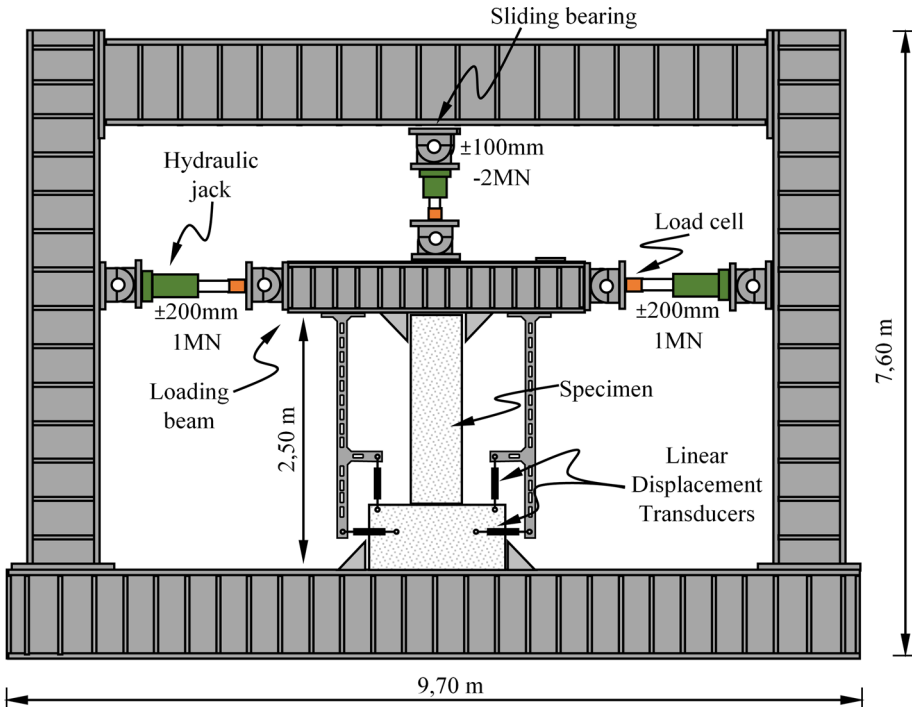
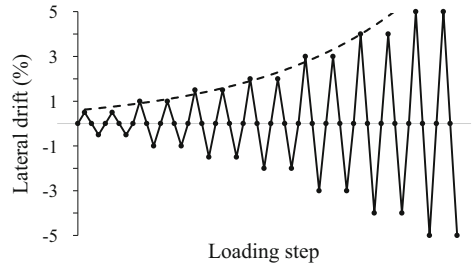


Fig. 6 Test setup

3 Test results

All specimens exhibited a flexural controlled response. No shear failure was observed. Damage state of the specimens at the end of the tests is represented in Figs. 7, 8, 9 and 10. The recorded lateral load-lateral displacement hysteretic behaviour for all specimens is presented in Fig. 11. Because the recorded response includes the second order effect caused by the large eccentricity of the axial load, the dotted lines in the charts in Fig. 11 should be referenced when the strength decay is analysed.

Cracking of specimen CIP1 was noticed at the first loading cycle to 0.25 % drift. At 0.5 % normal cracks spaced at 15–20cm covered the entire column height. Neutral axis depth at the bottom section of the column was around 20cm. After two loading cycles at ±2% no damage of the column was noticed. All the cracks were closed and no spalling of the concrete occurred (Fig. 7a). During the loading cycles to 4 % lateral drift, de-bonding cracks along the

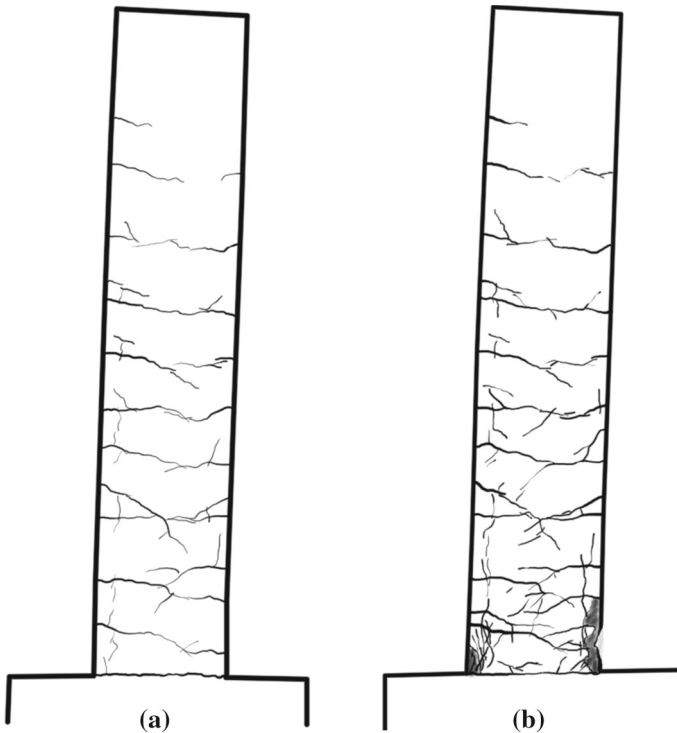


Fig. 7 Damage state of specimen CIP1 at 2 % (a) and 5 % (b) lateral drift

tensioned longitudinal reinforcement occurred in the plastic region of the column. Vertical cracking of the compressed concrete beyond the perimeter of the outer stirrups was noticed as well. Occurrence of these cracks subsequently caused the local spalling of the concrete cover which started during the second loading cycle to 4 % and amplified in the following cycles. Spalling of concrete was minor, the longitudinal reinforcement was not exposed and buckling did not occur. Damage state of specimen CIP1 at the end of the test, after two cycles at $\pm 5\%$, is represented in Fig. 7b. Failure of the specimen was not noticed.

The recorded lateral force—lateral displacement hysteretic response revealed a stable behaviour. No significant strength decay was observed. Severe pinching effect was observed for specimen CIP1.

Specimen CIP2 was similar to CIP1 but the applied axial load was doubled. Uniformly spaced cracks at around 20 cm occurred during the first loading cycle to 0.5 % lateral drift. The neutral axis depth decreased from $2/3$ of the effective depth, d , during the loading cycles to 0.5 % drift, to $1/3d$ after two cycles at 1 %. Extensive de-bonding cracks along the tensioned longitudinal reinforcement occurred during the loading cycles to 1.5 %. Vertical cracks in the compressed concrete was noticed in the subsequent cycles to 2 % drift. However, after two loading cycles at $\pm 2\%$, no significant damage of the specimen could be observed. Subsequent loading to 3 % lead to severe deterioration of the concrete cover followed by concrete spalling. The final damage state of the specimen (Fig. 8b) shows a clear plastic hinge location. No buckling of the longitudinal reinforcement was noticed.

The recorded hysteretic response shows a rather stable behaviour with minor strength decay. Pinching was noticed for this specimen as in case of CIP1, but the relative magnitude

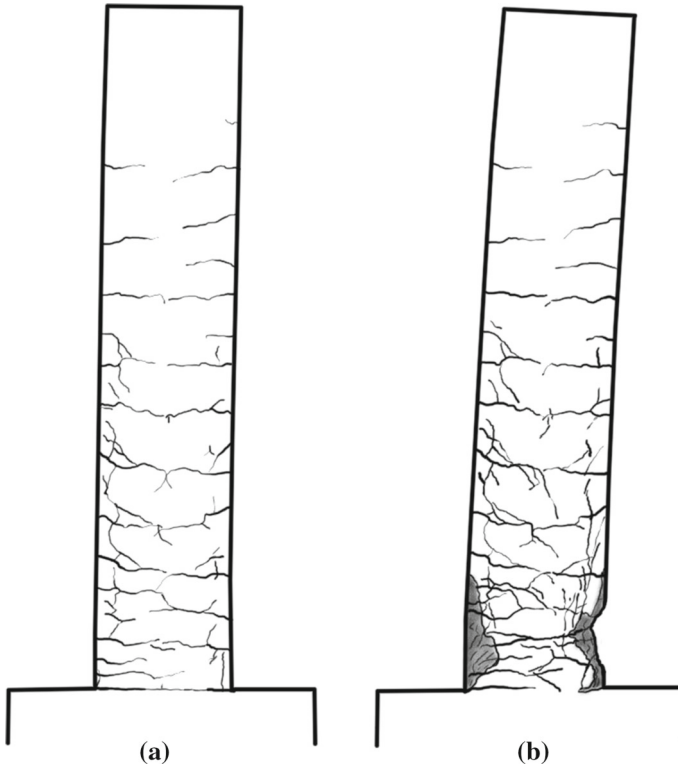


Fig. 8 Damage state of specimen CIP2 at 2% (a) and 5% (b) lateral drift

of the hysteretic energy loss caused by pinching was significantly lower. A behaviour analysis with respect to the dissipated energy for all specimens is presented in a subsequent paragraph.

A single crack appeared at the bottom of the column PC1 during the loading cycle to 0.25%. In the subsequent cycles at $\pm 0.5\%$ several normal cracks spaced at 15–20 cm occurred. At the bottom of the columns, two cracks spaced at 50 mm indicated the width of the grout layer. The length of the normal cracks extended over $2/3$ of the column effective depth after two loading cycles at $\pm 2\%$. No significant de-bonding cracks and no crushing of the compressed concrete or grout were noticed at this loading stage and the column was essentially undamaged. Subsequent loading caused the formation of a minor de-bonding crack along a $\phi 16$ mm longitudinal rebar at the corner of the column. Minor crushing of the grout layer was noticed as well. Most of the column rotation was concentrated at the bottom of the column. Two normal cracks developed at the limits of the grout layer. The response of the column resembles a rocking behaviour, most of the lateral deformation being caused by the rotation at the base of the column. No inclined cracks could be noticed. Damage state of the specimen is presented in Fig. 9. In case of specimen PC2, a similar behaviour was observed.

In comparison with the reference specimen CIP1, specimens PC1 and PC2 exhibited a slightly lower maximum lateral strength followed by no strength decay. The recorded pinching effect is more obvious. Hysteretic behaviour of these specimens is presented in Fig. 11b, c.

Specimen PC3 cracked during the initial loading cycles to 0.25% drift. A systematic cracking pattern appeared during the loading cycles to 0.5%. 30 cm uniformly spaced normal

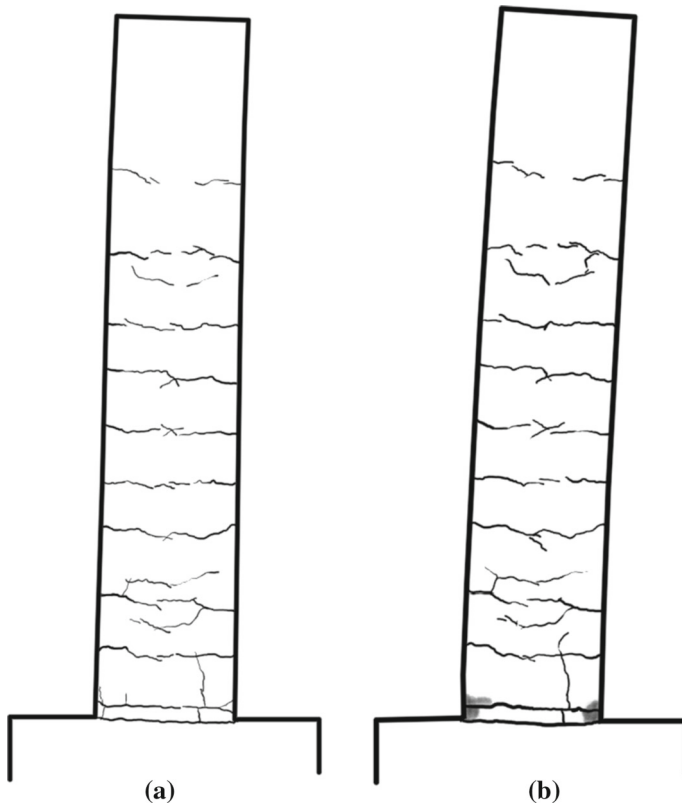


Fig. 9 Damage state of specimen PC1 at 2 % (a) and 5 % (b) lateral drift

cracks occurred. At 2 % lateral drift, only minor spalling of the grout layer was noticed and, essentially, the column had no significant damage. After 3 % lateral drift systematic vertical cracks appeared in the compressed area of the bottom part of column, both in the grout layer and the concrete. Moderate spalling of the grout and concrete was noticed and, eventually, the longitudinal rebars of the column were exposed. No significant de-bonding cracks could be observed up to 5 % drift. This can be explained by the increased amount of the longitudinal reinforcement in the plastic region due to overlapping. Lack of de-bonding cracks shows that tension in the longitudinal $\phi 16$ mm bars was moderate despite the use of a bottom steel plate anchorage system. A detailed analysis of strain variation in the reinforcement is presented in a subsequent paragraph. Similar behaviour was observed in case of specimen PC4. Damage state of these specimens at 5 % lateral drift is presented in Fig. 10.

In comparison with CIP2, moderate strength decay was noticed in case of specimens PC3 and PC4. This was caused mainly by the spalling of the compressed concrete and grout.

Pinching effect could be observed in case of all specimens. It was more obvious in case of specimens tested under lower axial stress, CIP1, PC1 and PC2.

In case of CIP1, pinching was caused by the severe tensile plastic strain of the longitudinal rebars unreversed during the compression loading cycles. The variation of strain in the corner rebars of specimen CIP1 with the lateral drift is presented in Fig. 12. During the early loading cycles to 0.5, 1.0 and 1.5 %, the distribution of strain in these rebars was linear, indicating

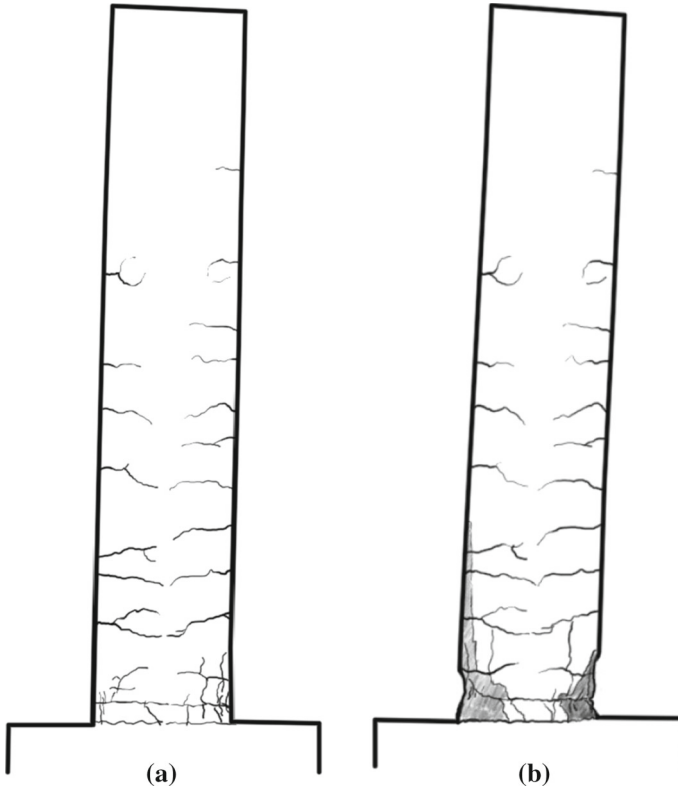


Fig. 10 Damage state of specimen PC3 at 2% (a) and 5% (b) lateral drift

an elastic response (Fig. 13). During the first loading cycle to 2%, severe yielding of the reinforcement in tension was recorded as can be seen in Figs. 12 and 13. After unloading, at zero lateral force, plastic tensile strain was still recorded in the longitudinal rebars. Loading in the opposite direction initially caused a partial reversion of this deformation. During this, the stiffness of the element was low because only the steel rebars were active in the compressed area. When the crack partially closed, the element was regaining its stiffness and the lateral load steadily increased up to yielding. This behaviour of the specimen reduced the energy dissipation capacity at large lateral deformation cycles. Forces in the compressed area of the column's cross-section were mainly supported by the longitudinal rebars preventing extensive damage of the column. Similar behaviour could be observed for specimen CIP2.

In case of PC specimens the strain in the longitudinal $\varphi 16$ mm rebars was rather low, with recorded values less than half of the yielding strain. An essentially constant strain distribution over the column height was recorded at each displacement peak. The recorded strain slowly increased with the lateral deformation. For example, the strain of the corner $\varphi 16$ mm rebars of specimen PC1 increased up to $1,200 \mu \varepsilon$ at the second loading cycle at 5% lateral drift. Basically, plastic strain occurred only in the $\varphi 25$ mm starter bars. The stress in these rebars was gradually transferred to the $\varphi 16$ mm bars of the column by overlapping. Above the grout layer, the rebar amount was essentially doubled by overlapping $4\varphi 25$ mm with $8\varphi 16$ mm. Analysis of the strain distribution in the $\varphi 16$ mm bars further emphasised that the plastic deformation was concentrated on a limited length in the $\varphi 25$ mm starter bars (Fig. 14).

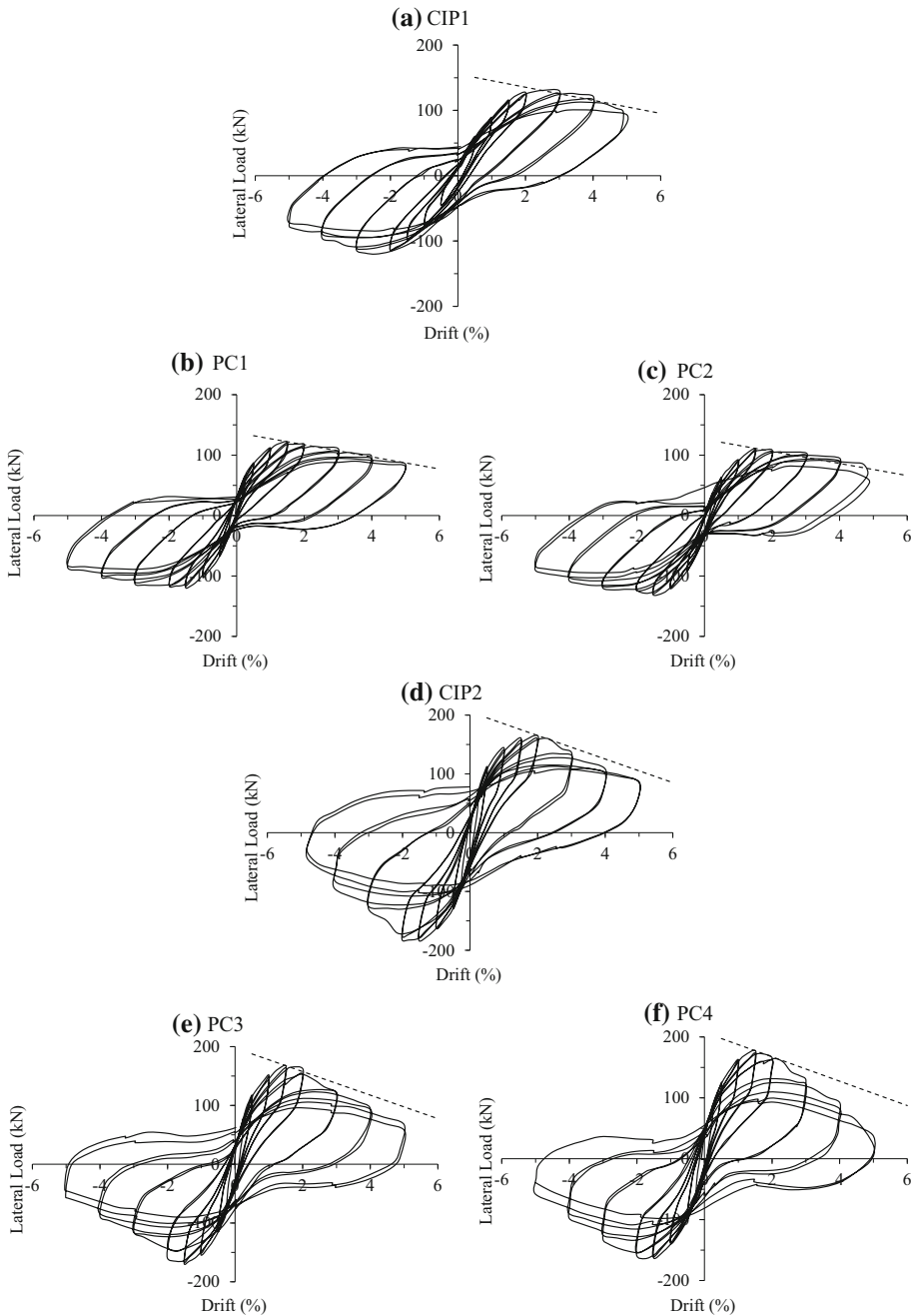


Fig. 11 Recorded hysteretic behavior

A similar hysteretic behavior of cast in place and precast specimens was observed. For each level of the applied axial load, the envelopes of the recorded hysteretic loops are essentially the same (Fig. 15).

Fig. 12 Specimen CIP1—variation of strain in the longitudinal reinforcement with the lateral drift

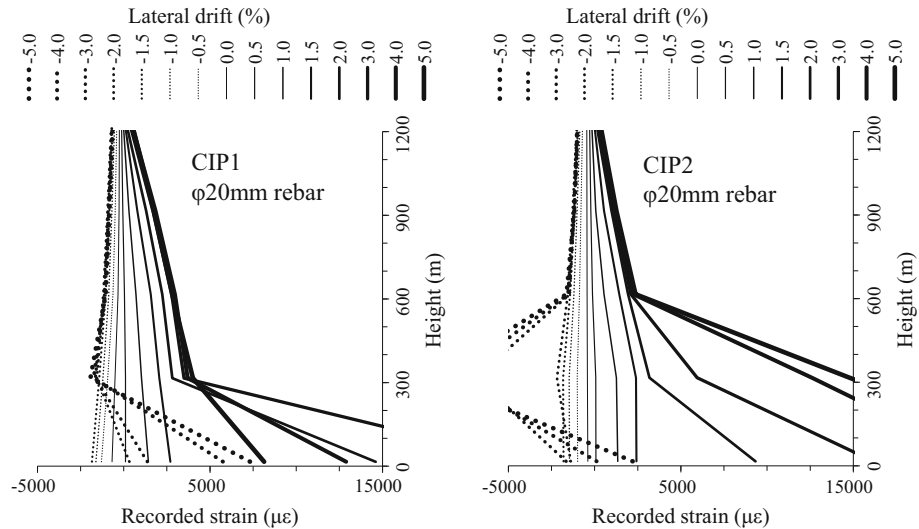
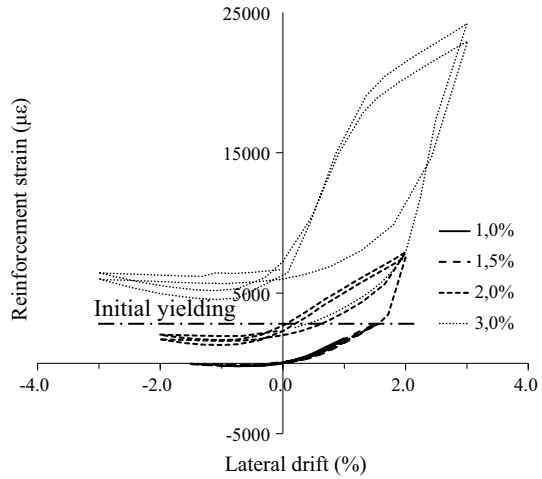


Fig. 13 Strain distribution in the longitudinal reinforcement at each displacement peak—CIP1 and CIP2

The hysteretic energy, calculated as the area enclosed by the hysteretic loops, for each pair of displacement cycles at 0.5, 1.0, 1.5, 2, 3, 4 and 5 %, resulted essentially the same for specimens CIP1, PC1 and PC2 (Fig. 16). Precast specimens dissipate roughly just 10 % more energy than the cast in place one at early displacement cycles, up to 2 % lateral drift, and 8 % less energy in the subsequent cycles. Overall, at the end of the loading tests CIP1 dissipated 8 % more energy than PC1 and 4 % more than PC2.

Similar behavior was observed in case of specimens tested under a 2,000kN axial load (Fig. 17). At the end of the loading tests, CIP 2 dissipated 7 % more energy than PC3 and 5 % more than PC4.

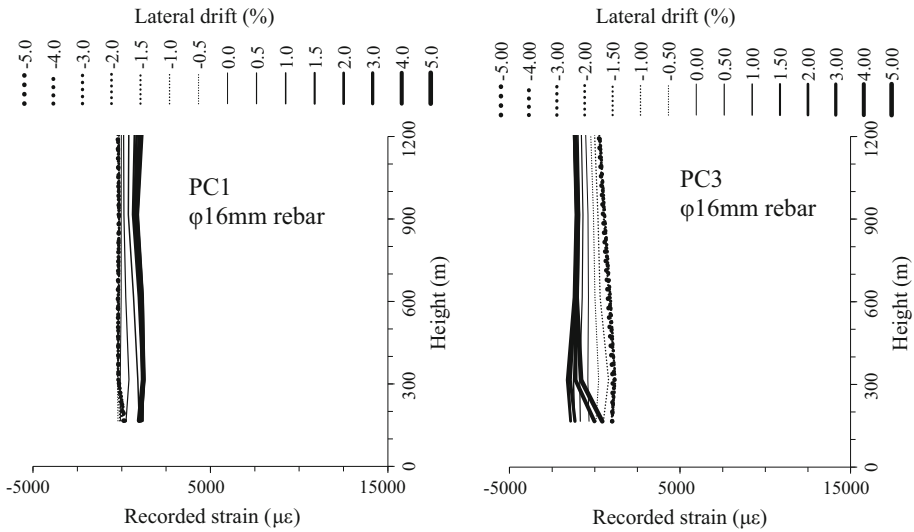


Fig. 14 Strain distribution in the longitudinal reinforcement at each displacement peak—PC1 and PC3

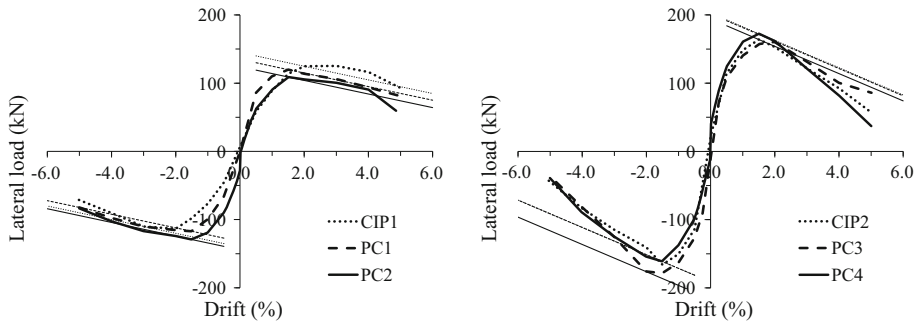


Fig. 15 Envelopes of the hysteresis loops

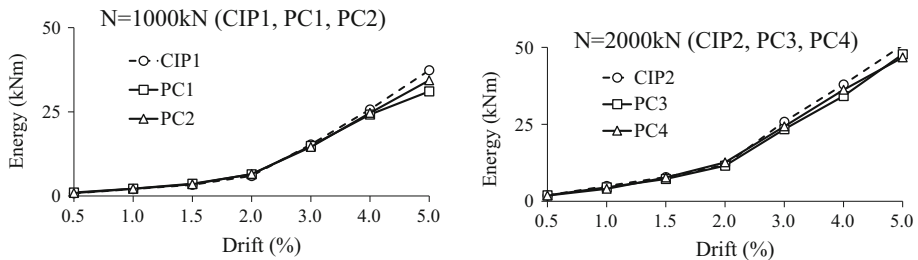


Fig. 16 Hysteretic energy for each pair of lateral displacement peaks

4 Evaluation of deformation capacity

Various models for the evaluation of the deformation capacity are available. In some models only the flexural response of the elements is accounted for (Sozen 2004; Paulay and Priestley 1992; Fardis and Biskinis 2003). It is assumed that after yielding a flexural failure mechanism

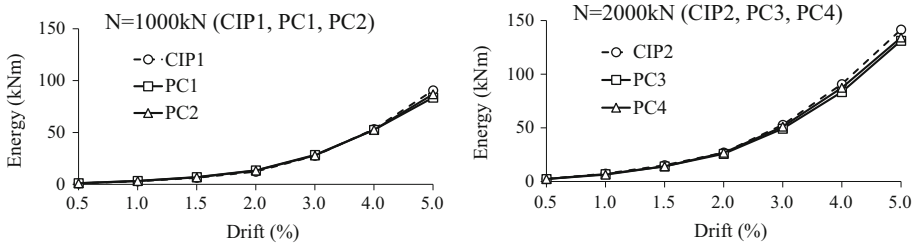


Fig. 17 Cumulated hysteretic energy at each lateral displacement peak

will occur. This assumption is usually suitable for slender columns with moderate axial loads. The combined action of bending and shear can reduce the shear strength of concrete members within few inelastic lateral deformation reversals. More elaborated deformation capacity models take into account the possibility of shear failure after the flexural yielding (Fardis and Biskinis 2003; Elwood and Moehle 2005; AIJ 1994).

The Structural Design Guidelines for Reinforced Concrete Buildings published by the Architectural Institute of Japan prescribe an analytical model for the evaluation of the deformation capacity for columns. This model takes into account the simultaneous contribution of the arch and truss action to the lateral strength of a concrete member. The validity of the model was confirmed based on a database of test results including compressed columns with transverse reinforcement ratios from 0 to 0.024, axial load ratios from 0 to 0.73 and concrete compressive strengths from 16.5 to 62.9 MPa.

Fardis and Biskinis introduced models for the deformation capacity of concrete members. Two of these models were incorporated into the European standard for seismic assessment of buildings, EN 1998-3 (CEN 2005). In one of the models (noted here F&B M1) the plastic component of the drift ratio is calculated as the product between the plastic component of the curvature and the plastic hinge length. The authors established empirical equations for computing the plastic hinge length to obtain results of the evaluation procedure for the ultimate drift ratio fitting experimental results from a large database of cast-in-place specimens. For each specimen, the deformation capacity was established based on the recorded hysteretic behaviour. As the authors found the predictive ability of this model unsatisfactory in some cases another model (noted here F&B M2) was developed, in which the chord rotation at flexure-controlled failure is calculated based on an empirical equation developed to fit experimental data. Both models include equations to determine the shear resistance that uses the ductility demand as an input parameter.

AIJ deformation capacity model was applied considering the characteristics of the reference specimens CIP1 and CIP2. The calculated shear strength of the columns decreases with the lateral inelastic displacement but it is higher than the flexural yielding strength for both specimens (Fig. 18). According to this model, shear failure doesn't occur either prior or after the flexural yielding of the columns. In this situation, the AIJ model cannot predict the ultimate displacement of the columns and a flexural response model should be used.

Fardis and Biskinis (2003) models estimated ultimate drift ratios larger than 5% for both columns. For specimen CIP1 a 10% ultimate drift ratio was computed using the model F&B M1 and 7% using F&B M2. The calculated load–drift relations represented in Fig. 19 include the second order effects caused by the large eccentricity of the axial loads. For specimen CIP2, both models estimated a roughly 6% ultimate drift ratio.

Evaluation using the Fardis and Biskinis models confirms the large deformation capacity of the tested specimens. Although the ultimate drift ratio could not be determined by

Fig. 18 Calculated response according to AIJ

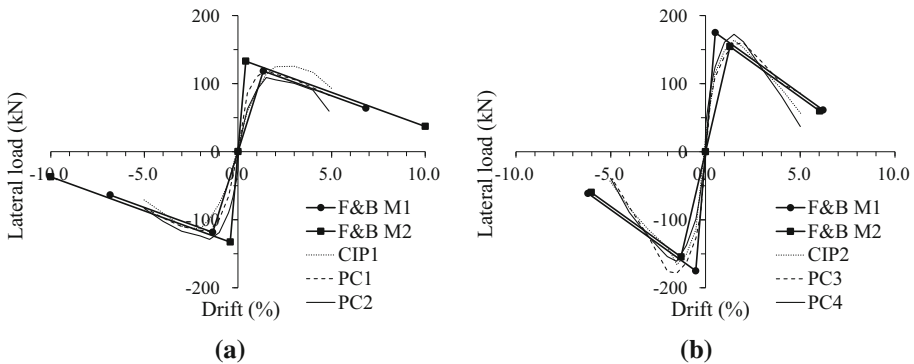
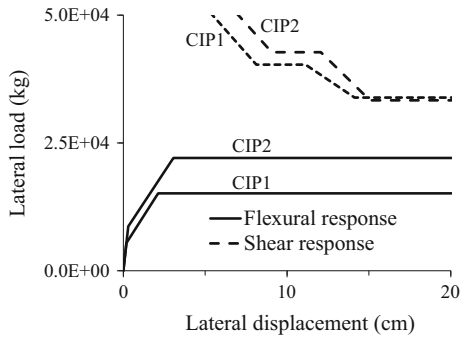


Fig. 19 Calculated deformation capacity according to Fardis and Biskinis (2003) models

tests, the calculated ultimate drift ratios are larger than maximum recorded values. The computed lateral load - lateral drift relations resemble the envelopes of the recorded hysteretic curves. In this experimental testing program, the precast specimens had similar hysteretic behaviour with the cast-in-place ones. Consequently, the Fardis and Biskinis models were considered suitable for the displacement capacity evaluation. The tested specimens are rather slender columns subjected to low to moderate axial loads. The suitability of these deformation capacity models for short columns with low concrete strength was previously reported by the authors (Popa et al. 2014).

5 Conclusions

A structural testing program was carried out to investigate the energy dissipation capacity of the connection of four precast concrete columns. For each precast specimen the connection between the column and the bottom stub was made using grouted corrugated steel sleeves. Two reference specimens with continuous longitudinal reinforcement from the bottom of the stubs to the top of the columns were tested as well. All the specimens were detailed for large ductility with limited amount of longitudinal reinforcement and considerable amount of transverse reinforcement in the critical region at the base of the column. Cyclic lateral displacement tests up to 5% lateral drift were performed under constant axial load. Two levels of axial load were considered, 1,000 and 2,000 kN, corresponding to average compressive

stresses of $0, 16f_{cd}$ and $0, 32f_{cd}$. For each level of axial load two precast specimens and one reference specimen were tested.

A similar hysteretic response was observed both for the precast and reference specimens for each level of applied axial force. Flexural or shear failure was not observed. All the specimens exhibited large ductility with minor strength decay. For each level of axial load, similar energy dissipation capacity was calculated for the precast and reference specimens. At the end of the loading cycles the reference specimens dissipated with 4–8 % more energy than the corresponding precast specimens.

Specimens tested with 1,000 kN axial load exhibited only minor damage. In case of the reference specimen, minor spalling of the concrete cover was noticed at 5 % lateral drift. Over 0.4 mm width flexural cracks were obvious at the bottom of the column. Splitting cracks were observed along the longitudinal rebars at the column corners indicating severe yielding of the steel. Spalling of the concrete did not uncover the rebars and no buckling of the rebars was observed. In case of the precast specimens, minor deterioration of the mortar bed was noticed. No spalling of the concrete in the columns was observed. Widely open flexural cracks were obvious at 5 % lateral drift at the limits of the grout layer. Minor and localized splitting cracks were observed along the longitudinal rebars.

Specimens tested with 2,000 kN axial load exhibited moderate damage. At 5 % lateral drift, moderate spalling of the concrete cover was observed. Longitudinal rebars were uncovered but no buckling was observed. Splitting cracks along the longitudinal rebars developed locally at the base of the column on a height roughly equal to the width of the concrete cross-section.

All the specimens showed minor damages at 2 % lateral drift, with no spalling of the concrete cover, limited splitting cracks and no deterioration of the mortar bed. The overall damage state for the precast specimens was less severe than the one of the reference specimens.

The results summarized above are valid for concrete columns with reinforcement layout, materials quality, aspect ratio and axial load ratio similar to the tested specimens. Further experimental studies are necessary to obtain relevant data based on which more comprehensive conclusions can be drawn. This experimental testing program showed that the grouted corrugated steel sleeves connections might be used for precast structures in seismic regions. For the tested specimens, the connections proved high rotational ductility and stable hysteretic response. If such connections are used, the structural analysis and design methodologies available for cast-in-place structures can be used in the design of precast structures. Special attention should be paid to the detailing of the transverse reinforcement to assure the required rotational ductility.

Acknowledgments The structural testing equipment was donated by Japanese Government through the Japanese International Cooperation Agency within the Technical Cooperation Project for Seismic Risk Reduction in Romania. This generous support is deeply acknowledged.

References

- ACI 318–11 (2011) Building code requirements for structural concrete. ACI Standard, Reported by ACI Committee 318, Farmington Hills, Michigan
- ACI 374.1 (2013) Guide for testing reinforced concrete structural elements under slowly applied simulated seismic loads. ACI Standard, Reported by ACI Committee 374, Farmington Hills, Michigan
- ACI 550.1 (2009) Guide to emulating cast-in-place detailing for seismic design of precast concrete structures. ACI Standard, Reported by Joint ACI-ASCE Committee 550, Farmington Hills, Michigan, ISBN: 9780870313196
- AIJ (1994) AIJ Structural design guideline for reinforced concrete buildings. Tokyo

- Arslan MH, Korkmaz HH, Gulay FG (2006) Damage and failure pattern of prefabricated structures after major earthquakes in Turkey and shortfalls of the Turkish Earthquake code. *Eng Fail Anal* 13(4):537–557. doi:[10.1016/j.engfailanal.2005.02.006](https://doi.org/10.1016/j.engfailanal.2005.02.006)
- Belleri A, Riva P (2012) Seismic performance and retrofit of precast concrete grouted sleeve connections. *PCI J* 57(1):97–109
- Bournas D, Negro P, Taucer F (2014) Performance of industrial buildings during the Emilia earthquakes in Northern Italy and recommendations for their strengthening. *Bull Earthq Eng* 12:2383–2404. doi:[10.1007/s10518-013-9466-z](https://doi.org/10.1007/s10518-013-9466-z)
- Bruneau M (2002) Building damage from the Marmara, Turkey earthquake of August 17, 1999. *J Seismol* 6:357–372
- CEN (2004a) Eurocode 2: design of concrete structures—part 1-1: general rules and rules for buildings. European Standard EN 1992-1-1, Brussels
- CEN (2004b) Eurocode 8: design of structures for earthquake resistance—part 1: general rules, seismic actions and rules for buildings. European Standard EN 1998-1, Brussels
- CEN (2005) Eurocode 8: design of structures for earthquake resistance—part 3: assessment and retrofitting of buildings. European Standard EN 1998-3, Brussels
- Elwood KJ, Moehle JP (2005) Drift capacity of reinforced concrete columns with light transverse reinforcement. *Earthq Spectra* 21(1):71–89. doi:[10.1193/1.1849774](https://doi.org/10.1193/1.1849774)
- Fardis MN, Biskinis DE (2003) Deformation capacity of RC members, as controlled by flexure or shear. Proceeding. In: Kabeyasawa T, Shiohara H (eds) Performance-based engineering for earthquake resistant reinforced concrete structure. Department of Architecture, University of Tokyo, Tokyo, pp 511–530
- FEMA (2007) Interim testing protocols for determining the seismic performance characteristics of structural and non-structural components, Report No. FEMA 461. Washington DC, US
- Ghosh SK, Cleland M (2012) Observations from the February 27, 2010, earthquake in Chile. *PCI J* 57(1):52
- Liberatore L, Sorrentino L, Liberatore D, Decanini L (2013) Failure of industrial structures induced by the Emilia (Italy) 2012 earthquakes. *Eng Fail Anal* 34:629–647. doi:[10.1016/j.engfailanal.2013.02.009](https://doi.org/10.1016/j.engfailanal.2013.02.009)
- Ministry of Regional Development and Public Administration of Romania (2013) Seismic design code. Part 1—design provisions for buildings, P100-1/2013. Bucharest
- Ozden S, Erdogan H, Akpınar E, Atalay HM (2014) Performance of precast concrete structures in October 2011 Van earthquake, Turkey. *Mag Concr Res* 66(11):543–552. doi:[10.1680/mac.13.00097](https://doi.org/10.1680/mac.13.00097)
- Paulay T, Priestley MJN (1992) Seismic design of reinforced concrete and masonry buildings. Wiley, New York
- Posada M, Wood SL (2002) Seismic performance of precast industrial buildings in Turkey. In: 7th National conference on earthquake engineering, 7NCEE, Boston, 21–25 July 2002
- Popa V, Cotofana D, Vacareanu R (2014) Effective stiffness and displacement capacity of short reinforced concrete columns with low concrete quality. *Bull Earthq Eng*. doi:[10.1007/s10518-014-9618-9](https://doi.org/10.1007/s10518-014-9618-9)
- Sozen MA (2004) Seismic behavior of reinforced concrete buildings. In: Bozorgnia Y, Bertero VV (eds) Earthquake engineering: from engineering seismology to performance-based engineering. CRC Press, Boca Raton, pp 13.1–13.41